CFTR modulator response measurements in subjects with cystic fibrosis using 2D differentiated nasal epithelia converted into spheroids

Gimano D. Amatngalim [1,2,*], Lisa W. Rodenburg [1,2], Bente L. Aalbers [3], Henriette H. M. Raeven [1,2], Ellen M. Aarts [1,2], Iris A.L. Silva [4], Wilco Nijenhuis [5], Sacha Vrendenbarg [1,2], Evelien Kruisselbrink [1,2], Jesse E. Brunsveld [1,2], Cornelis M. van Drunen [6], Sabine Michel [1], Karin M. de Winter-de Groot [1], Harry G. Heijerman [3], Lukas C. Kapitein [5], Magarida D. Amaral [4], Cornelis K. van der Ent [1], Jeffrey M. Beekman [1,2]

[1] Department of Pediatric Pulmonology, Wilhelmina Children's Hospital, University Medical Center Utrecht, Utrecht University, member of ERN-LUNG, Utrecht, the Netherlands.

[2] Regenerative Medicine Center Utrecht, University Medical Center Utrecht, Utrecht University, Utrecht, the Netherlands.

[3] Department of Pulmonology, University Medical Center Utrecht, Utrecht, the Netherlands.

[4] BioISI-Biosystems & Integrative Sciences Institute, Faculty of Sciences, University of Lisboa, Lisboa, Portugal.

[5] Cell Biology, Neurobiology and Biophysics, Department of Biology, Faculty of Science, Utrecht University, Utrecht, Netherlands.

[6] Department of Otorhinolaryngology, Amsterdam University Medical Centers, University of Amsterdam, Amsterdam.

***Correspondence:** G.D.Amatngalim@umcutrecht.nl

Summary

Cystic Fibrosis (CF) is caused by genetic defects that impair the cystic fibrosis transmembrane conductance regulator (CFTR) channel in airway epithelial cells. These defects may be overcome by specific CFTR modulating drugs, for which the efficacy can be determined in a personalized manner using 3D nasal-brushing-derived airway spheroids in a forskolin-induced swelling (FIS) assay. Despite of this, previously described culture methods and application of 3D airway spheroids in CFTR function assays have not been fully optimal. In this report we describe an alternative method of culturing nasal airway spheroids, which are derived from an equally differentiated airway epithelial monolayer of a 2D air-liquid interface culture. Optimized spheroid culture conditions, enabled consistent detection of CFTR modulator responses in nasal spheroids from subjects with CF, including the highly effective CFTR triple modulator combination therapy VX-661/VX-445/VX-770.

Keywords: Cystic fibrosis, Cystic Fibrosis Transmembrane Conductance Regulator, Nasal epithelium, 3D spheroids, Personalized medicine

48 **Introduction**

49 Cystic fibrosis (CF) is a monogenic epithelial disease caused by mutations in the cystic fibrosis
50 conductance transmembrane regulator (*CFTR*) gene [1]. This defect impairs CFTR-dependent
51 anion conductance in airway epithelia [2], which leads to a severe respiratory disease[3]. CFTR
52 modulators are target-specific drugs that may restore CFTR function in individuals with CF [4].
53 However, the efficiency of modulators largely depends on the CFTR genotype of an individual
54 with CF. More than 2,000 distinct CFTR mutations have been reported
55 (http://www.genet.sickkids.on.ca//) with variable effects on CFTR expression or function. In
56 addition to common mutations, such as the F508del allele, approximately 1,000 rare mutations
57 have been identified that each affect less than 5 individuals worldwide. This low prevalence
58 makes it unfeasible to determine CFTR modulator drug efficacy in large cohort clinical studies.
59 As an alternative of determining drug efficacy directly in individuals with CF, the effects of
60 CFTR modulators can be predicted using patient-derived epithelial cultures in functional CFTR
61 assays [5]. This is traditionally done with 2D air-liquid interface (ALI)-differentiated airway
62 epithelia by assessment of CFTR-dependent chloride (Cl^-) currents via electrophysiology [6–8] or
63 via indirect measurements of CFTR, such as quantification of ciliary function, airway surface
64 liquid depth, or pH [9–11]. However, a major disadvantage of the ALI-culture model system is
65 the limited scalability. In contrast, CFTR-expressing epithelial organoids/spheroids from
66 various tissues, i.e. airway, intestine, kidney, are emerging as a novel model system in which
67 drug efficacy can be tested more efficiently in a mid-to high-throughput fashion [12–14].
68 Previously, we and others have shown that intestinal organoids from subjects with CF can be
69 used to predict drug responses in a forskolin-induced swelling (FIS) assay, reflecting CFTR-
70 dependent fluid secretion [15–18]. Nevertheless, based on the origin of CF respiratory disease, it
71 remains postulated that airway epithelial models are more predictive for determining CFTR
72 modulator responses.

Indeed, we previously reported CFTR modulator response measurements in long-term expanded distal airway organoids using FIS [14]. However, we observed large variations in FIS measurements, as swelling was limited to well-differentiated spherical structures. Others have successfully used 3D airway spheroids derived from minimal-invasive nasal brushings in functional CFTR assays [19–21], which are a more suitable option for personalized drug testing compared to cultures derived from invasive (tracheo)bronchial and intestinal tissues. However, previously described functional CFTR assays using nasal spheroids were either low-in throughput or required CFTR function measurements over extensive time periods [19–21]. Altogether, there is a remaining need for a further optimized and scalable FIS assay using nasal airway spheroids, which enables efficient CFTR modulator response measurements in subjects with CF.

In this work, we therefore describe an alternative approach of culturing 3D nasal brushing-derived airway spheroids and optimal culture conditions for CFTR modulator response measurements. We first isolate and expand human nasal airway epithelial cells (HNEC), followed by differentiation in 2D ALI-cultures. Subsequently, fragments of a uniform differentiated ALI-culture derived monolayer are embedded in Matrigel, leading to conversion into 3D airway spheroids. Due to initial lack of CFTR modulator responses in nasal spheroids of individuals with CF and a F508del/F508del genotype, we further optimized spheroid culture conditions by including the growth factor/cytokine combination neuregulin-1β and IL-1β. Validation studies using this culture condition showed consistent detection of CFTR modulator responses in CF nasal spheroid FIS measurements, including repairing effects of the FDA-approved CFTR triple modulator therapy VX-661/VX-445/VX-770 [22].

98 **Results**

99

100 **Characterization of nasal-brushing-derived 2D airway epithelial cell cultures.**

101 We first optimized the culture procedures for human nasal epithelial cells (HNEC) derived from
102 nasal brushings (Figure 1A). We isolated and expanded brushing-derived HNEC in 2D cell
103 cultures (Figure 1B) using a growth factor-defined and feeder layer-free culture medium (Table
104 S1), integrating culture components from previously described culture protocols [23–26]. HNEC
105 stained positive for p63 and cytokeratin 5 (KRT5), confirming a basal cell phenotype (Figure
106 1C). After expansion, HNEC were cryo-stored to enable repeated usage of donor materials. We
107 further cultured defrosted and expanded HNEC till passage 4-6, followed by differentiation in
108 conventional 2D ALI-cultures, to recapitulate the mucociliary airway epithelium. This was
109 done using a defined differentiation medium (Table S2) based on previous reports [27,28].
110 Differentiated ALI-cultures displayed significant lower mRNA expression of basal cell markers
111 and enhanced expression of secretory and ciliated cell markers compared to undifferentiated
112 controls (Figure S1A). In addition, ALI-HNEC displayed a differentiation-dependent increase
113 in trans-epithelial electrical resistance and ciliogenesis (Figure S1B, and C). Well-differentiated
114 ALI-HNEC cultures resembled the native nasal epithelial tissue, by displaying a similar
115 pseudostratified morphology and consisting of luminal MUC5AC^{+} goblet cells, β-tubulin IV^{+}
116 ciliated cells, and retaining p63^{+} and KRT5^{+} basal cells (Figure 1D). This was furthermore
117 confirmed by whole mount imaging, showing expression of the secretory cell markers
118 MUC5AC, CC10, and basal cell marker p63 at the apical and basal side respectively (Figure
119 1E). CFTR function and effects of modulators were confirmed in ALI-HNEC from healthy
120 controls (HC) and individuals with CF and a F508del/F508del genotype (CF F508del/F50del).
121 This was done by two independent research laboratories via short-circuit and open-circuit Cl^{-}
122 current measurements respectively (Figure S1D-F).

123

124 **Conversion of differentiated ALI-HNEC into 3D nasal spheroids and use in FIS assays.**

125 We previously reported CFTR function measurements in distal airway organoids using a FIS
126 assay [14]. However, in this study we observed large variation in swelling between individual
127 organoids, which was restricted to large spherical structures. This is likely caused by the
128 unsynchronized differentiation of individual organoids, which may influence differentiation-
129 dependent CFTR function (Figure S2). To overcome this heterogeneity, we developed an
130 alternative method in which 3D nasal airway spheroids are derived from 2D differentiated ALI-
131 HNEC cultures. In this method, a differentiated monolayer of an ALI-culture is first dissociated
132 from the transwell membrane, followed by disruption and embedding of small epithelial
133 fragments in Matrigel droplets. The differentiated epithelial fragments self-organized into
134 spheroids within 48 h, with the lumen located at the inside of the structures (Figure 1F). This
135 was confirmed by visual observation of beating cilia and accumulation of mucus (Video S1),
136 as well as by immunofluorescence imaging, demonstrating β-tubulin IV^{+} cilia and MUC5AC^{+}
137 secretory cells inside of the spheroid, and p63^{+} and KRT5^{+} basal cells at the basal side (Figure
138 1G, H). Next, we determined whether ALI-derived nasal spheroids could be used to measure
139 CFTR function in FIS assays (Figure 2A). Forskolin stimulation of spheroids from HC subjects
140 increased swelling in time, which was dose-dependent and reached a plateau at 5 μM forskolin
141 (Figure 3B-D). FIS measured in nasal spheroids from HC subjects was significantly higher
142 compared to subjects with CF (Figure 3E, F), thereby demonstrating that HC and CF spheroids
143 can be distinguished phenotypically based on FIS. In contrast, HC and CF nasal spheroids both
144 displayed cystic lumens, and were not significant different in size (Figure 3G, H). Chemical
145 CFTR inhibitors only partially inhibited FIS in HC nasal spheroid cultures, while CF nasal
146 spheroids displayed a significant increase in swelling upon forskolin stimulation, despite CFTR
147 dysfunction (Figure S3A-D). Overall, this suggests partial CFTR-independent fluid secretion

148 in nasal spheroids. To further examine CFTR-independent swelling, we determined the effect
149 of the Ca^{2+}-activated Cl^- channel (CaCC) activator E_{act} [29] in nasal spheroid swelling.
150 Interestingly, E_{act} induced a more significant swelling response in CF nasal spheroids compared
151 to HC cultures (Figure 2I and J). E_{act} has been shown to increase cellular uptake of Ca^{2+} via
152 transient receptor potential cation channel subfamily V member 4 (TRPV4), a protein which,
153 similar to CFTR, can be activated in a cAMP/PKA-dependent manner [30,31]. In line with these
154 findings and in part explaining CFTR-independent FIS, HC and CF nasal spheroid swelling,
155 induced by the cAMP-enhancing compound forskolin, was partially and completely suppressed
156 respectively upon TRPV4 inhibition (Figure S3E). Next to TRPV4, we further assessed
157 inhibition of the CaCC ANO1 (TMEM16A), which however did not reduce FIS in CF nasal
158 spheroids (n=2 independent donors) (Figure S3F).
159
160 **Neuregulin and IL-1β improve CFTR modulator responses in CF nasal spheroids.**
161 Although CF and HC spheroids could be distinguished phenotypically based on FIS, we did not
162 observe repairing effects of the CFTR corrector and potentiator combination VX-809/VX-770
163 in CF F508del/F508del nasal spheroids from multiple subjects (Figure 3A and B). Therefore,
164 we aimed to optimize CFTR modulator response measurements, by modifying the spheroid
165 culture conditions. This was done by examining a panel of growth factors and cytokines, which
166 were added after plating of the epithelial fragments and during spheroid culturing (Figure 3C).
167 The examined factors included, neuregulin-1β (NR), which has been reported to enhance
168 epithelial polarization and differentiation of secretory cells in ALI-cultures [32,33]. Moreover, the
169 effect of the pro-inflammatory cytokine IL-1β was examined, which has been shown to enhance
170 CFTR mRNA expression, chloride currents, and CFTR modulator responses in ALI-cultures
171 [34–38]. In contrast to independent factors, a combination of NR/IL-1β reduced CFTR-independent
172 FIS and resulted in a clear detection of VX-809/VX-770 modulator responses in CF

173 F508del/F508del nasal spheroids (Figure 3D and Figure S4A). NR/IL-1β-cultured HC
174 spheroids displayed a similar swelling response compared to control culture conditions (Figure
175 3E and S4B). In further support of attenuating CFTR-independent fluid secretion, NR/IL-1β
176 attenuated lumen formation in CF nasal spheroids, as quantitated by spheroid size
177 measurements (Figure 3F, G). This effect could be attributed to IL-1β (Figure S4C). Also partly
178 explaining improved CFTR modulator responses, NR/IL-1β increased mRNA expression of
179 *CFTR*, whereas expression of the Ca^{2+} activated chloride channel *ANO1* and Cl^- channel
180 *SLC26A9* were reduced and enhanced respectively (Figure 3H). In contrast, NR/IL-1β did not
181 affect the expression of mucociliary differentiation markers (Figure 3H and S4D). Next, we
182 further validated FIS measurements in the NR/IL-1β culture condition, by examining a larger
183 cohort of HC and CF subjects. HC nasal spheroid cultures displayed a significant higher
184 swelling response when compared to cultures from CF F508del/F508del subjects (Figure 4A,
185 B, and D). Moreover, the CFTR modulator combination VX-809/VX-770 consistently
186 enhanced FIS measured in CF F508del/F508del spheroid cultures from 7 independent subjects
187 (Figure 4C and D, S5A). In addition to VX-809, FIS responses in CF F508del/F508del
188 spheroids (n=1 donor) were modulated upon treatment with other CFTR correctors (Figure
189 S5B). We were also able to detect VX-770 potentiator responses in nasal spheroids from
190 subjects with CF and a S1251N gating mutation (Figure S5C-E). Moreover, the novel highly
191 effective CFTR triple modulator therapy VX-445/VX-661/VX-770 [22], induced a high increase
192 in FIS measurements in CF F508del/F508del spheroids cultured with NR/IL-1β (Figure
193 4E,F,G). VX-445 by itself did not increase FIS, whereas chemical CFTR inhibition completely
194 diminished increases in swelling by VX-445/VX-661/VX-770, demonstrating CFTR-
195 dependence of the modulator treatment effect (Figure S5F and G).
196
197

198 **Discussion**

199 In this report, we describe a new method of culturing nasal brushing-derived airway spheroids,
200 which can be used in a functional CFTR assay to quantify target-specific drug responses. To
201 overcome the unsynchronized differentiation observed in previously reported 3D airway
202 organoids [14], we setup up a novel approach in which evenly differentiated spheroids are
203 established from ALI-differentiated airway epithelial monolayers. This approach was based on
204 our experience with culturing airway organoids from resected tissues, in which we observed
205 that tissue-derived epithelial fragments self-organize into organoids within a few days after gel
206 embedding. Based on this observation and the assumption that ALI-cultures reflect the
207 differentiated airway epithelia tissue, we proposed that epithelial fragments from 2D-cultures
208 could be converted into 3D spheroids as well. Indeed, embedding of differentiated ALI-derived
209 epithelial fragments in Matrigel led to formation of spheroids, which directly displayed a
210 differentiated phenotype. From a single 12 mm^2 transwell insert we are able to generate a yield
211 of spheroids that is sufficient for 48 independent wells (approx. 25-50 spheroids/well) of a 96
212 well plate used in FIS assays. In terms of scalability, this demonstrates a major advantage of
213 our method compared to the conventional use of 2D ALI-cultures.

214 As previously reported with other CFTR-expressing organoids/spheroids [12–14], fluid secretion
215 can be quantified in ALI-derived nasal spheroid swelling using a FIS assay. Although, we were
216 able to discriminate HC from CF nasal spheroids cultures based on FIS, further characterization
217 studies suggested a role of CFTR-independent fluid secretion in mediating spheroid swelling.
218 This was in part explained by studies using an activator (E_{act}) and inhibitor of TRPV4,
219 demonstrating a role of Ca^{2+} in mediating CFTR-independent fluid secretion. Interestingly, E_{act}-
220 induced swelling was significant higher in CF nasal spheroids compared to HC controls,
221 suggesting enhanced CFTR-independent fluid secretion upon CFTR dysfunction. We were
222 unable to reduce spheroid swelling with a specific inhibitor of the CaCC ANO1. This suggests

223 the involvement of another chloride channel in mediating CFTR-independent FIS. The partial
224 and lack of effects of chemical CFTR and ANO1 inhibitors might also be due the inefficient
225 penetration of the compounds to the apical surface of the spheroids. Further research is therefore
226 required to gain further insight into the mechanism underlies CFTR-independent fluid secretion
227 in nasal spheroids. For instance, by more accurate gene knock-out studies using CRISPR gene
228 editing.
229 We were initially unable to detect effects of the CFTR modulators VX-809/VX-770 in CF
230 F508del/F508del nasal spheroids, likely due to high CFTR-independent FIS and low CFTR
231 expression. Therefore, we optimize the spheroid culture conditions by including NR/IL-1β. In
232 support of enhanced CFTR specificity, NR/IL-1β reduced CFTR-independent swelling, while
233 increasing and reducing the expression of CFTR and CaCC ANO1 respectively. Alterations in
234 ion channel expression corresponded with a recent study showing similar outcomes in IL-1β
235 stimulated ALI-cultured airway epithelial cells [37]. The Cl^- channel SLC26A9 was also increased
236 upon stimulation with NR/IL-1β, which may support CFTR function, as proposed by others [39].
237 The NR/IL-1β culture condition likely reflects the chronically inflamed airway epithelium of
238 individuals with CF, and therefore act as physiological conditions for testing CFTR modulator
239 responses in nasal spheroids. However, further research is required to determine whether
240 NR/IL-1β also improve CFTR modulator responses in other airway model systems, such as
241 distal airway organoids, or other CFTR-expressing epithelial cells.
242 We further validated the NR/IL-1β spheroid culture conditions using multiple FDA-approved
243 CFTR modulating drugs. In addition to consistent responses to VX-809/VX-770 in CF
244 F508del/F508del nasal spheroids, this included the highly effective CFTR modulator therapy
245 VX-445/VX-661/VX-770, in line with promising clinical outcomes [22]. In both the initially
246 tested spheroid culture conditions and the optimized conditions with NR/IL-1β, we could not
247 discriminate HC from CF spheroids based on lumen size, which is in contrast to the CFTR-

248 dependent intestinal organoid model [12,16]. Another limitation of our study is the low number of
249 donors used in several experiments. Furthermore, due to limited numbers of donors with diverse
250 CFTR genotypes, we were furthermore unable to determine whether residual FIS correlated to
251 disease severity, as shown by others [21]. The potential clinical impact of our method will be
252 determined in follow up studies, in which we will explore whether CFTR modulator responses
253 in ALI-derived nasal spheroids are predictive for therapy efficacy in individuals with CF, and
254 how this correlates with other *in vitro* measurements, i.e. intestinal organoids and 2D ALI-
255 differentiated nasal/bronchial airway epithelial cultures [8,15,40]. Furthermore, our method may
256 be used to examine novel target-specific therapies for subjects with CF with unmet, such as
257 assessment of CRISPR-gene editing, read-through agents, or compounds targeting nonsense
258 mediated decay. Moreover, complementary to 2D ALI-cultures, our novel airway spheroid
259 culture method may potentially be further used to model other respiratory diseases.
260
261
262
263
264
265
266
267
268
269
270
271
272

Acknowledgments

This work was supported by grants of the Dutch Cystic Fibrosis Foundation (NCFS, HIT-CF grant); Netherlands Organization for Health Research and Development (ZonMw); Health Holland (grant no 40-41200-98-9296); SRC 013 from CF Trust-UK; UIDB/04046/2020 and UIDP/04046/2020 centre grants (to BioISI), both from FCT/MCTES Portugal; and "HIT-CF" (H2020-SC1-2017-755021) from EU. This work is supported by the European Research Council (ERC Consolidator Grant 819219 to L.C.K.).

Author Contributions

Conception and/or design: GA, LR, CE, JMB; Acquisition, analysis, or interpretation of data: GA, LR, HR, EA, IS, WN, SV, BA, EK, JEB, SM, KW, HH, LK, MA, CE, JMB; Drafting the work or revising it critically for important intellectual content: GA, CD, MA, CE, JMB; Final approval of the version submitted for publication; GA, LR, HR, EA, IS, WN, SV, BA, EK, JEB, CD, SM, KW, HH, LK, MA, CE, JMB.

Competing Interests

JMB has a patent granted (10006904) related to CFTR function measurements in organoids and received personal fees from HUB/ Royal Dutch academy of sciences, during the conduct of the study; non-financial support from Vertex Pharmaceuticals, and personal fees and non-financial support from Proteostasis Therapeutics, outside the submitted work. CE reports grants from GSK, Nutricia, TEVA, Gilead, Vertex, ProQR, Proteostasis, Galapagos NV, Eloxx pharmaceuticals, outside the submitted work; In addition, CE has a patent related to CFTR function measurements in organoids (10006904) with royalties paid. MA reports grants and personal fees from Vertex Pharmaceuticals, grants from Gilead Sciences, Inc., grants and

personal fees from Proteostasis Therapeutics, personal fees from Translate Bio MA, Inc, during the conduct of the study.

322 **Figure Legends**

323

324 **Figure 1) Conversion of differentiated ALI-HNEC cultures into 3D nasal airway**
325 **spheroids.** (A) Graphic illustration of workflow showing isolation and differentiation of nasal
326 brushing-derived HNEC, followed by conversion into 3D nasal spheroids. (B) Brightfield
327 images of a HNEC expansion culture. (C) Immunofluorescent (IF) staining of HNEC with basal
328 cell markers p63 (red) and cytokeratin 5 (KRT5, green). (D) Sections of nasal tissue (top) and
329 18 days differentiated ALI-HNEC (bottom), demonstrating IF staining of MUC5AC (goblet
330 cells, red), β-tubulin IV (ciliated cells, green), p63 and KRT5 (both basal cell markers, green
331 and red respectively). (E) Whole-mount IF confocal images of ALI-HNEC differentiated for 18
332 days, showing maximal projections of the apical side of the secretory cell markers MUC5AC
333 and Club Cell protein 10 (CC10), and ciliated cell marker β-tubulin IV (Z-stack at the bottom).
334 The projection of the basal side shows the basal cell marker p63 (Z-stack at the bottom). All
335 epithelial markers are shown in green. (F) Time course showing self-organization of
336 differentiated ALI-HNEC-derived epithelial fragments into spheroids. (G) IF staining of nasal
337 spheroids for β-tubulin IV, MUC5AC, and p63 (all in green). H) Confocal images showing in
338 the top panels staining with DAPI (blue), β-tubulin IV (green), and MUC5AC (red). The bottom
339 panels show staining with DAPI (blue), p63 (green), and KRT5 (red). DAPI (blue) was used as
340 nuclear staining (C-E, G, and H). Phalloidin (red) was used as actin cytoskeleton staining (E
341 and G). See also Figure S1, S2 and Supplemental Video 1.

342

343 **Figure 2) Forskolin-induced swelling assay with ALI-culture derived nasal spheroids.** (A)
344 Graphic illustration showing FIS assay with ALI-derived nasal spheroid cultures. (B)
345 Representative brightfield images (top) and images of calcein green acetoxymethyl (AM)
346 esters-strained (bottom) spheroids from a HC subject, which were unstimulated (Control) or

347 treated with forskolin (Fsk, 5 μM). Images were taken at t=0, 60, and 120 min after stimulation.
348 (C and D) Nasal spheroids from HC subjects (n=5 independent donors) were stimulated with
349 different concentrations of Fsk (0-10 μM), followed by quantification of FIS. (E and F)
350 Comparison between HC and CF nasal spheroid swelling (both n=8 independent donors) after
351 Fsk, (5 μM) stimulation. (G) Representative brightfield images of nasal spheroids from HC
352 subjects and subjects with CF. (H) Quantification of the mean spheroid area (μm^2, means ± SD)
353 of HC and CF spheroids (both n=6 independent donors). (I and J) Comparison between HC and
354 CF nasal spheroid swelling (both n=6 independent donors) after stimulation with the calcium-
355 activated chloride channel agonist E_{act} (10 μM). Results are depicted as the percentage change
356 in surface area relative to t=0 (normalized area) measured at 15-minute time intervals for 2 h
357 (means ± SD) (C, E, I), and area under the curve (AUC) plots (t=120 min, means ± SD) (D, F,
358 J). Analysis of differences was determined with a one-way ANOVA and Bonferroni *post-hoc*
359 test (D), and unpaired t-test (F, H, J). ** $p<0.01$, *** $p<0.001$, **** $p< 0.0001$. See also Figure
360 S3.
361
362 **Figure 3) Optimization of CFTR modulator response measurements with NR/IL-1β.**
363 (A and B) CF F508del/F508del nasal spheroids (n=8 independent donors) were pre-treated with
364 VX-809 or vehicle control for 48 h. Subsequently, FIS was determined after acute stimulation
365 with Fsk, (5 μM), together with VX-770 or vehicle control. (C) Illustration showing culturing
366 of nasal spheroids with NR/IL-1β. (D) CF F508del/F508del nasal spheroids (n=3 independent
367 donors) were cultured at control conditions, or stimulated with neuregulin (NR, 0.5 nM),
368 interleukin-1β (IL-1β, 10 ng/ml), or combination (NR+IL-1β) for 5 days. At day 3, cultures
369 were pre-treated with VX-809 or vehicle control for 48 h, and afterwards acutely stimulated
370 with forskolin (Fsk, 5 μM) in combination with VX-770 or vehicle control before measuring
371 FIS. (E) Assessment of FIS in HC spheroids (n=3 independent donors) cultured under control

372 conditions or with NR+IL-1β for 5 days. FIS assay results are depicted as the percentage change
373 in surface area relative to t=0 (normalized area) (means ± SD) (A), and area under the curve
374 (AUC) plots (t=120 min, means ± SD) (B, D, E). (F) Brightfield images of CF F508del/F508del
375 nasal spheroids cultured in control conditions or with NR+IL-1β for 5 days. (G) Quantification
376 of the mean spheroid area (μm^2, means ± SD) of control and NR+IL-1β cultured CF
377 F508del/F508del spheroids (n=3 independent donors). (H) mRNA expression analysis of CF
378 F508del/F508del nasal spheroids (n=3-6 independent) that were left unstimulated (Control) or
379 cultured with NR+IL-1β for 5 days. mRNA expression was determined of *CFTR*, *ANO1*,
380 *SLC26A9,* (all chloride channels), *SPDEF* (secretory cells) and *FOXJ1* (ciliated cells). Results
381 represent target mRNA expression normalized for the geometric mean expression of the
382 housekeeping genes *ATP5B* and *RPL13A* (means ± SD). Analysis of differences was
383 determined with an unpaired t-test (B, E) and paired t-test (D, G, H). * $p<0.05$, ** $p<0.01$. See
384 also Figure S4.
385
386 **Figure 4) Validation of CFTR modulator responses in NR/IL-1β-cultured nasal spheroids.**
387 (A) Brightfield images (top) and images of calcein green AM-stained (bottom) nasal spheroids
388 cultured with NR/IL-1β, showing FIS in HC and CF F508del/F508del cultures. Images were
389 taken at t=0, and 120 min. (B-D) Swelling of (B) HC nasal spheroids (n=5 independent donors)
390 and (C) CF F508del/F508del spheroids (n=7 independent donors) cultured with NR/IL-1β. HC
391 nasal spheroids were left untreated (control) or stimulated with Fsk (5 μM). CF nasal spheroids
392 were first pre-treated with VX-809 or vehicle for 48 h, before stimulation with Fsk in
393 combination with VX-770 or vehicle. (E) Images of calcein green AM-stained CF
394 F508del/F508del spheroids cultured with NR/IL-1β. Spheroids were pre-treated with vehicle
395 (top panels) or triple CFTR modulator combination VX-661/VX-445 (bottom panels) for 48 h,
396 before acute stimulation with Fsk in combination with VX-770 or vehicle control. Images were

397 taken at t=0, and 120 min. (F and G) CF F508del homozygous nasal spheroids cultured with
398 NR/IL-1β (n=4 independent donors) were pre-treated with vehicle, VX-661 or a combination
399 of VX-661 and VX-445 for 48 h. Swelling was determined afterwards following acute
400 stimulation with Fsk together with VX-770 or vehicle. Swelling results are depicted as (B,C,F)
401 the percentage change in surface area relative to t=0 (normalized area) measured at 15-minute
402 time intervals for 2 h (means ± SD), and (D,G) area under the curve (AUC) plots (t=120 min,
403 means ± SD). Analysis of differences was determined with a paired t-test (D; within groups,
404 G), unpaired t-test (D; HC compared to CF)., ** $p<0.01$, *** $p<0.001$, **** $p< 0.0001$. See
405 also Figure S4 and S5.
406
407
408
409
410
411
412
413
414
415
416
417
418
419
420
421

422 # Methods

423

424 ## Resources Table

425

Reagent or Resource	Source	Identifier
Antibodies		
Mouse IgG1 anti-β-tubulin IV	Emergo Biogenex	#MU178-UC
Rabbit anti-β-tubulin IV	Abcam	#ab179509
Rabbit anti-MUC5AC	Abcam	#ab198294
Rabbit anti-P63	Abcam	#ab124762
Mouse IgG1 anti cytokeratin 5	Abcam	#ab17130
Mouse IgG1 anti-CC10	Acris, Origene	#AM26360PU-N
Goat anti-Mouse IgG1, Alexa Fluor 488	Invitrogen	#A-21121
Goat anti-Mouse IgG1, Alexa Fluor 647	Invitrogen	#A-21240
Goat anti-Rabbit IgG, Alexa Fluor 488	Invitrogen	#A-11034
Goat anti-Rabbit IgG, Alexa Fluor 546	Invitrogen	#A-11035

Biological Samples		
Nasal brushings	UMC Utrecht	Protocol ID: 16/586, NL54885.041.16
Nasal turbinate tissue	Academic Medical Center Amsterdam	N/A
Chemicals, Peptides, and Recombinant Proteins		
TrypLE express enzyme	Fisher scientific	# 12605010
Sputolysin	Calbiochem	#560000-10
Collagen IV	Sigma-Aldrich	#C7521
CryoStor® CS10	StemCell Technologies	#07930
PureCol	Advanced BioMatrix	#5005
Bronchial epithelial cell medium-basal (BEpiCM-b)	Sciencell	#3211
Advanced DMEM F12	Thermo Fisher	#12634-028
B-27 Supplement, serum free	Thermo Fisher	#12587010
GlutaMAX Supplement	Thermo Fisher	#35050-061
HEPES	Thermo Fisher	#15630080
(±)-Epinephrine hydrochloride	Sigma-Aldrich	#E4642
Hydrocortisone	Sigma-Aldrich	#H0888

3,3′,5-Triiodo-L-thyronine sodium salt	Sigma-Aldrich	#T6397
N-Acetyl-L-cysteine	Sigma-Aldrich	#A9165
Nicotinamide	Sigma-Aldrich	#N0636
SB02190	Sigma-Aldrich	#S7067
DMH-1	Selleck Chemicals	#S7146
A83-01	Tocris	#2939/10
Y-27632	Selleck Chemicals	#S1049
DAPT	Fisher Scientific	#15467109
TTNPB	Cayman	#16144-1
Recombinant human FGF-7	Peprotech	#100-19
Recombinant human FGF-10	Peprotech	#100-26
Recombinant human EGF	Peprotech	#AF-100-15
Recombinant human HGF	Peprotech	#100-39H
Recombinant Neuregulin-1β	Peprotech	#100-03
Recombinant Interleukin 1β	Peprotech	#200-01B
Penicillin-Streptomycin	Thermo Fisher	#15070-063
Primocin	Invivogen	#ant-pm-2
Amphotericin B	Thermo Fisher	#15290018

Gentamicin	Sigma-Aldrich	#G1397
Vancomycin	Sigma-Aldrich	#SBR00001
Collagenase type II	Thermo Fisher	#17101-015
CFTRinh-172	Sigma-Aldrich	#C2992
GlyH101	Sigma-Aldrich	#219671
VX-809	Selleck Chemicals	# S1565
VX-661	Selleck Chemicals	#S7059
VX-770	Selleck Chemicals	#S1144
Correctors C1-18	Cystic Fibrosis Foundation Therapeutics	https://www.cff.org/Research/Researcher-Resources/Tools-and-Resources/CFTR-Chemical-Compound-Program/
Forskolin	Sigma-Aldrich	#F3917
Ani9	Sigma-Aldrich	# SML1813
Benzamil	Sigma-Aldrich	# B2417
RN-1734		#R0658
3-Isobutyl-1-methylxanthine	Sigma-Aldrich	# I5879
Amiloride	Sigma-Aldrich	#1019701
Calcein green acetoxymethyl (AM)	Invitrogen	#C34852
Alexa Fluor 555 Phalloidin	Invitrogen	#A34055
Phalloidin-iFluor 405	Abcam	#ab176752
Prolong Gold antifade reagent	Thermo Fischer	#P36934

Prolong Gold antifade reagent with DAPI	Thermo Fischer	#P36935
iQ SYBR Green Supermix	Bio-Rad	#1708880
Critical Commercial Assays		
RNeasy Mini Kit	Qiagen	#74104
iScript cDNA synthesis kit	Bio-Rad	#1708891
Experimental Models: Cell Lines		
Human nasal airway epithelial cells (HNEC)	This paper	N/A
Hek293T – R-spondin-1 mFc cell line	Trevigen Cat# 3710-001-	N/A
Oligonucleotides		
Primers used for this manuscript		Table S4
Equipment		
Zeiss LSM800 confocal microscopy	Zeiss	N/A
Leica SP8X confocal microscope	Leica	N/A
Leica THUNDER imager	Leica	N/A

Leica TCS SP8 STED 3X microscope	Leica	N/A
Ussing chamber system	Physiologic Instruments	N/A
Voltage clamp	World Precision Instruments	#DVC-1000
PowerLab	AD Instruments	#8/30
Epithelial voltohmmeter EVOM2	World Precision Instruments	N/A
Nanodrop spectrophotometer	Thermo Fisher	N/A
CFX96 real-time detection machine	Bio-Rad	N/A
Software and Algorithms		
Zen Blue Software	Zeiss	https://www.zeiss.com/microscopy/int/products/microscope-software/zen.html
Prism 8	GraphPad Software Inc.	https://www.graphpad.com/scientific-software/prism/
Microsoft Excel	Microsoft Corporation	https://office.microsoft.com/excel
Adobe Illustrator	Adobe	https://www.adobe.com/nl/products/illustrator.html
LabChart 6	AD Instruments	https://labchart.software.informer.com/6.0/
CFX Manager 3.1	BioRad	https://www.bio-rad.com/en-us/sku/1845000-cfx-manager-software?ID=1845000
LAS X software	Leica	https://www.leica-microsystems.com/products/microscope-software/p/leica-las-x-ls/
ImageJ/FIJI		https://imagej.net/Fiji/Downloads

Others		
Cytological brush	CooperSurgical	#C0004
12 mm Transwell® with 0.4 µm Pore Polyester Membrane Insert	Corning	#3460
6.5 mm Transwell® with 0.4 µm Pore Polyester Membrane Insert	Corning	#3470
Matrigel	Corning	#354230
BC isolation and expansion medium		Table S1
Air-liquid interface differentiation medium		Table S2
Airway spheroid culture medium		Table S3

426

427 **Patient materials and sample collection**

428 Nasal brushings were collected from healthy volunteers without respiratory tract symptoms
429 (n=22 independent donors), and subjects with CF (n=22 independent donors) by a trained
430 research nurse or physician, essentially as previously described [41]. Sampling of adults was
431 conducted using a cytological brush and without anesthetics. Nasal brushings of infants (<6
432 years old) were collected with a modified interdental brush [42]. Samples were taken from the
433 inferior turbinates of both left and right nostrils and stored in collection medium, consisting of
434 advanced (ad)DMEM/F12, with GlutaMAX (1% v/v), HEPES (10 mM), Penicillin-

435 Streptomycin (1% v/v), and Primocin (100 µg/mL). Nasal brushings were collected and stored
436 with informed consent of all participants and was approved by a specific ethical board for the
437 use of biobanked materials TcBIO (Toetsingscommissie Biobanks), an institutional Medical
438 Research Ethics Committee of the University Medical Center Utrecht (protocol ID: 16/586).
439 Nasal samples from infants with CF were collected as part of the Precision study (protocol ID:
440 NL54885.041.16), which was approved by the Medical Research Ethics Committee of the
441 University Medical Center Utrecht (Utrecht, The Netherlands). Resected inferior nasal
442 turbinate tissue was obtained from a subject who underwent corrective surgery for turbinate
443 hypertrophy at the Academic Medical Center in Amsterdam, the Netherlands. The tissue was
444 accessible for research within the framework of patient care, in accordance with the "Human
445 Tissue and Medical Research: Code of conduct for responsible use" (2011) (www.federa.org),
446 describing the no-objection system for coded anonymous further use of such tissue without
447 necessary written or verbal consent.

448

449 **Isolation and expansion of human nasal airway epithelial cells as 2D-cultures**

450 Nasal cells were dissociated from the brush in the collection medium by scraping through a
451 sterile P1000 pipette tip with the top cut off. After centrifugation (400 g for 5 min), the pellet
452 was treated with TrypLE express enzyme, supplemented with 1x Sputolysin. The cells were
453 incubated for 10 min at 37 ºC and strained using a 100 µm strainer. After centrifugation (400 g
454 for 5 min), the remaining pellet was used for isolation of human nasal epithelial cells (HNEC).
455 HNEC were isolated and expanded on 6-well culture plates coated with collagen IV (50 µg/mL)
456 and using BC isolation and expansion medium (Table S1) respectively. BC isolation medium
457 contained additional antibiotics to suppress microbial outgrowth and was used during the first
458 week of epithelial cell isolation, before switching to BC expansion medium. BC expansion

459 medium included the gamma-secretase inhibitor DAPT, which reduces outgrowth of squamous
460 cells at late passages. Growth factors (FGF7, FGF10, EGF, and HGF) were added freshly to the
461 culture medium. Cultures were refreshed three times a week (Monday, Wednesday, Friday).
462 After reaching 80-90% confluency, cells were passaged with TrypLE express enzyme and
463 further expanded for one passage before freezing with CryoStor® CS10, supplemented with Y-
464 27632 (5 µM) to create a master cell bank. For further use, a work cell bank was created of
465 passage 2 cells, which was cryo-stored before further use.

466

467 **Differentiation of 2D ALI-HNEC cultures**

468 Expanded HNEC (passage =4-6) were cultured on transwell inserts (0.4 µm pore size polyester
469 membrane), which were coated with PureCol (30 µg/mL). Cells were seeded in a density of 0.2
470 or $0.5*10^6$ cells on 24 or 12 wells inserts respectively and cultured in submerged conditions in
471 BC expansion medium until reaching confluency. Afterwards, culture medium was changed
472 with air-liquid interface (ALI)-differentiation medium (Table S2) supplemented with A83-01
473 (500 nM), and cells were additionally cultured in submerged condition for 1-2 days.
474 Subsequently, culture medium at the apical side was removed and cells were further
475 differentiated as ALI-cultures. After 3-4 days, cells were refreshed with ALI-diff medium
476 without additional A83-01 and differentiated for at least 14 additional days at ALI-conditions.
477 Medium was refreshed twice a week (Monday and Thursday or Tuesday and Friday), and the
478 apical side of the cultures was washed with PBS once a week. The trans-epithelial electrical
479 resistance (TEER) was measured with an epithelial voltohmmeter (EVOM2), to determine the
480 airway epithelial barrier integrity of ALI-HNEC cultures during differentiation. The mean
481 resistance was corrected for the surface area of the transwell insert (⌀ 6.5 mm) and depicted as
482 $\Omega*cm^2$.

483

484 **Conversion of 2D differentiated ALI cultures into airway spheroids**

485 Differentiated ALI-cultures were washed at the apical surface with PBS and subsequently
486 treated at the basolateral side with collagenase type II (1 mg/mL) diluted in adDMEM/F12.
487 Cultures were incubated at 37 ºC and 5% CO_2 for 45-60 min until the epithelium detaches from
488 the transwell insert. Next, the dissociated epithelial layer was transferred to a 15 ml tube in 1
489 ml adDMEM/F12 + 10 % (v/v) Fetal bovine serum (FBS), mechanically disrupted into smaller
490 fragment by pipetting, and strained with a 100 µm filter. After centrifugation (at 400 g, 5 min),
491 the epithelial pellet was resuspended in ice-cold 75% growth factor reduced Matrigel (v/v in
492 airway spheroid (AS) medium Table S3). Next, epithelial fragments were embedded in 30 µl
493 Matrigel droplets on pre-warmed 24-well suspension plates. Droplets were solidified at 37 ºC
494 and 5% CO_2 for 20-30 min, before adding 0.5 ml AS medium (Table S3). In optimized
495 conditions for measuring CFTR modulator responses, AS culture medium was further
496 supplemented with neuregulin-1β (NR, 0.5 nM) and interleukin-1β (IL-1β; 10 ng/ml). Besides,
497 NR/IL-1β we furthermore examined the effects of culturing with other interleukins i.e. IL-13,
498 IL-4, IL-10, and the growth factors: fibroblast growth factor 2, 7, 10, hepatocyte growth factor,
499 and insulin-like growth factor 1, which did not improve the detection of CFTR modulator
500 responses (*data not shown*). AS medium was refreshed twice a week (Monday and Thursday
501 or Tuesday and Friday).

502

503 **Forskolin-induced swelling (FIS) assay**

504 ALI-derived nasal airway spheroids were used in forskolin-induced swelling (FIS) assays,
505 essentially as previously described with minor adaptation [14,43]. In short, airway spheroids were
506 transferred 3-5 days after conversion in 96-well plates in 4 µl droplets of 75% matrigel (v/v in

507 AS medium), containing approx. 25-50 structures. After solidification of droplets, 100 µl AS
508 medium was added to each well. In optimized conditions for measuring CFTR modulator
509 responses, AS culture medium was supplemented with neuregulin-1β (0.5 nM) and interleukin-
510 1β (10 ng/ml). Spheroid swelling was conducted in quadruplicates. In indicated experiments,
511 spheroid cultures were pre-treated with CFTRinh-172 and GlyH101 (CFTRi, both 50 µM),
512 Ani9 (ANO1i; 10 µM), or RN-1734 (TRPV4i; 10 µM) or vehicle as negative control, for 4 h.
513 CFTR correctors: VX-809, VX-661 (both 10 µM), VX-445 (5 µM), C1-18 (all 10 µM) or
514 vehicle were pre-treated for 48 h. Before assessment of FIS, spheroid cultures were stained with
515 Calcein green AM (3 µM) for 30 min. Afterwards, spheroids were stimulated with forskolin
516 with indicated concentration. In cultures from subjects with CF, the CFTR potentiator VX-770
517 (10 µM) or vehicle was added together with forskolin. Swelling of nasal spheroids was
518 quantitated by measuring the increase of the total area of calcein green AM-stained spheroids
519 in a well during 15-min time intervals for a period of 2 h. Images were acquired with a Zeiss
520 LSM800 confocal microscopy, using a 2.5 or 5x objective and experiments were conducted at
521 37°C and 95% O_2/5% CO_2 to maintain a pH of 7.4. Data was analysed using Zen Blue Software
522 and Prism 8.
523

524 **Ussing chamber experiments**

525 Short-circuit current (Isc) measurements were conducted with an Ussing chamber system using
526 a voltage clamp using differentiated ALI-HNEC, cultured on transwell inserts (⌀ 6.5 mm).
527 Electrophysiological analyses were carried out along an apical-to-basolateral Cl^- gradient to
528 maximize apical CFTR function measurements, by using a basolateral buffer consisting of 120
529 mM NaCl, 25 mM $NaHCO_3$, 3.33 mM KH_2PO_4, 0.83 mM K_2HPO_4, 1.2 mM $CaCl_2.H_2O$ and
530 1.2 mM $MgCl_2.6H_2O$, and apical buffer consisting of 1.2 mM NaCl, 25 mM $NaHCO_3$, 3.33
531 mM KH_2PO_4, 0.83 mM K_2HPO_4, 1.2 mM $CaCl_2$.H2O and 1.2 mM $MgCl_2$.6H2O and 141 mM

532 Na-gluconate. During measurement, ALI-HNEC were sequentially stimulated with Benzamil
533 (5 µM, apical side) to block epithelial Na^+ channel-mediated currents, The CFTR potentiator
534 VX-770 (5 µM, apical/basolateral side, only in VX-809 treated CF ALI-HNEC), followed by a
535 mix of cAMP agonist forskolin/IBMX (10 µM /100 µM, apical/basolateral side), and the
536 specific CFTR channel blocker CFTRInh-172 (5 µM, apical side). Measurements were
537 conducted at a bath temperature of 37°C and continuously gassing with 95% O_2/5% CO_2 to
538 maintain a pH of 7.4. Tracings were recorded and analyzed with PowerLab and LabChart 6.

539 For open circuit measurements, transwell inserts (⌀ 12 mm) were mounted in the chamber
540 device and continuously perfused at the apical and basal side with a Ringer solution of the
541 following composition (mmol/L) 145 NaCl, 1.6 K_2HPO_4, 1 $MgCl_2$, 0.4 KH_2PO_4, 1.3 Ca^{2+}
542 Gluconate and 5 Glucose, and pH adjusted to 7.4. Following a 20 min stabilization period
543 amiloride (20µM) was added to the apical side to block epithelial Na^+ channel-mediated
544 currents, followed by forskolin/IBMX (2µM/100µM), VX-770 (3µM) and CFTRInh-172
545 (30µM) were added sequentially. Transepithelial Voltage (V_{te}) values were recorded at all times
546 with Power Lab software (AD Instruments Inc.). Values for V_{te} were referred to the basal side
547 of the epithelium and transepithelial resistance (R_{te}) was determined by applying short
548 intermittent pulses (0.5 µA/s), measuring pulsated deviations in V_{te} and accounting for the area
549 of the inserts. An empty insert was previously recorded to correct the measured values. Short-
550 circuit currents (I_{eq-sc}) were calculated according to Ohm's law from V_{te} and R_{te} (I_{eq-}
551 $_{sc} = V_{te} / R_{te}$).

552

553 **RNA extraction, cDNA synthesis, and quantitative real time PCR**

554 Total RNA was extracted from ALI-cultures using the RNeasy Mini Kit according to the
555 manufacturer's protocol. RNA yield was determined by a Nanodrop spectrophotometer and
556 subsequently cDNA was synthesized by use of the iScript cDNA synthesis kit according to the
557 manufacturer's protocol. Quantitative real-time PCR (qPCR) was performed with specific
558 primers (Table S4) using the iQ SYBR Green Supermix and a CFX96 real-time detection
559 machine. CFX Manager 3.1 software was used to calculate relative gene expression normalized
560 to the housekeeping genes *ATP5B* and *RPL13A* according to the standard curve method.

561

562 **Immunofluorescence staining and microscopy**

563 2D expanded HNEC and ALI-HNEC cultures were fixed in 4% paraformaldehyde for 15 min,
564 permeabilized in 0.25% (v/v) Triton-X in PBS for 30 min and treated with blocking buffer,
565 consisting of 1% (w/v) BSA and 0.25% (v/v) Triton-X in PBS, for 60 min. Next, primary
566 antibodies (1:500) in blocking buffer were added at the apical side and incubated for 1-2 h or
567 overnight. Afterwards, cells were washed three times with PBS and incubated with secondary
568 antibodies and Phalloidin (1:500) in blocking buffer for 30 min in dark, followed by three
569 washings in PBS. Transwell membranes were subsequently cut from the inserts and placed on
570 slides. All samples were mounted with Prolong Gold antifade reagent with or without DAPI.
571 Resected nasal tissue and ALI-HNEC cultures were fixed with 4 % paraformaldehyde and
572 embedded in paraffin after dehydration. After deparaffinization followed by antigen retrieval
573 using citrate buffer (pH = 6) for 20 min, the 5 µm sections were permeabilized in 0.25% (v/v)
574 Triton-X in PBS for 15 min, then treated with blocking buffer, consisting of 5% (w/v) BSA and
575 0.025% (v/v) Triton-X in PBS, for 30 min. Primary antibodies in blocking buffer, were
576 incubated for 2 h, followed by incubation of secondary antibodies for 1 h. Samples were
577 mounted with Prolong Gold reagent with DAPI. Spheroids plated in 4 µl droplets of 75%
578 matrigel (v/v) in a 96 wells plate, were fixed with 4 % paraformaldehyde for 10 min, and stained

579 as previously described [14,44], using indicated primary antibodies. Images were acquired with a
580 Leica SP8X confocal microscope, Leica THUNDER imager, and Leica TCS SP8 STED 3X
581 microscope. Images were processed using LAS X software and ImageJ/FIJI.
582
583 **Quantification and statistical analysis**
584 Swelling assays were conducted in quadruplicates for each experimental condition, and results
585 are shown as mean ± SEM of independent subjects. Increases in the total surface area of a
586 spheroids in a single well is calculated as normalized swelling, relative to t=0, which is set as
587 baseline of 100%. For swelling assays, statistical analysis was assessed with area under the
588 curve (AUC) values (t=120 min). Analysis of differences was determined with a one/two-way
589 repeated measurements ANOVA and Bonferroni *post-hoc* test or (un)paired Student's t-test as
590 indicated in the figure legends. Normal distribution was tested using the Shapiro Wilk test.
591 Differences were considered significant at $p < 0.05$. Statistical analysis was conducted using
592 Prism 8 (GraphPad Software Inc.).
593
594 **Data and Software Availability**
595 All data is provided with the manuscript.
596
597
598
599
600
601
602
603

604 **References**

605

606 1. Riordan, J.R., Rommens, J.M., Kerem, B., Alon, N., Rozmahel, R., Grzelczak, Z.,
607 Zielenski, J., Lok, S., Plavsic, N., and Chou, J.L. (1989). Identification of the cystic
608 fibrosis gene: cloning and characterization of complementary DNA. Science *245*,
609 1066–1073.

610 2. Knowles, M.R., Stutts, M.J., Spock, A., Fischer, N., Gatzy, J.T., and Boucher, R.C.
611 (1983). Abnormal ion permeation through cystic fibrosis respiratory epithelium.
612 Science *221*, 1067–1070.

613 3. Stoltz, D.A., Meyerholz, D.K., and Welsh, M.J. (2015). Origins of Cystic Fibrosis
614 Lung Disease. N. Engl. J. Med. *372*, 351–362.

615 4. Boyle, M.P., and De Boeck, K. (2013). A new era in the treatment of cystic fibrosis:
616 correction of the underlying CFTR defect. Lancet Respir. Med. *1*, 158–163.

617 5. Clancy, J.P., Cotton, C.U., Donaldson, S.H., Solomon, G.M., VanDevanter, D.R.,
618 Boyle, M.P., Gentzsch, M., Nick, J.A., Illek, B., Wallenburg, J.C., et al. (2019). CFTR
619 modulator theratyping: Current status, gaps and future directions. J. Cyst. Fibros. Off.
620 J. Eur. Cyst. Fibros. Soc. *18*, 22–34.

621 6. Gentzsch, M., Boyles, S.E., Cheluvaraju, C., Chaudhry, I.G., Quinney, N.L., Cho, C.,
622 Dang, H., Liu, X., Schlegel, R., and Randell, S.H. (2017). Pharmacological Rescue of
623 Conditionally Reprogrammed Cystic Fibrosis Bronchial Epithelial Cells. Am. J.
624 Respir. Cell Mol. Biol. *56*, 568–574.

625 7. Awatade, N.T., Uliyakina, I., Farinha, C.M., Clarke, L.A., Mendes, K., Solé, A.,
626 Pastor, J., Ramos, M.M., and Amaral, M.D. (2015). Measurements of Functional

627 Responses in Human Primary Lung Cells as a Basis for Personalized Therapy for
628 Cystic Fibrosis. EBioMedicine *2*, 147–153.

629 8. Pranke, I.M., Hatton, A., Simonin, J., Jais, J.P., Le Pimpec-Barthes, F., Carsin, A.,
630 Bonnette, P., Fayon, M., Stremler-Le Bel, N., Grenet, D., et al. (2017). Correction of
631 CFTR function in nasal epithelial cells from cystic fibrosis patients predicts
632 improvement of respiratory function by CFTR modulators. Sci. Rep. *7*, 7375.

633 9. Saint-Criq, V., Haq, I.J., Gardner, A.I., Garnett, J.P., Ward, C., Brodlie, M., and Gray,
634 M.A. (2019). Real-Time, Semi-Automated Fluorescent Measurement of the Airway
635 Surface Liquid pH of Primary Human Airway Epithelial Cells. J. Vis. Exp.

636 10. Choi, H.-C., Kim, C.S.K., and Tarran, R. (2015). Automated acquisition and analysis
637 of airway surface liquid height by confocal microscopy. Am. J. Physiol. Lung Cell.
638 Mol. Physiol. *309*, L109-18.

639 11. Chioccioli, M., Feriani, L., Kotar, J., Bratcher, P.E., and Cicuta, P. (2019). Phenotyping
640 ciliary dynamics and coordination in response to CFTR-modulators in Cystic Fibrosis
641 respiratory epithelial cells. Nat. Commun. *10*, 1763.

642 12. Dekkers, J.F., Wiegerinck, C.L., de Jonge, H.R., Bronsveld, I., Janssens, H.M., de
643 Winter-de Groot, K.M., Brandsma, A.M., de Jong, N.W.M., Bijvelds, M.J.C., Scholte,
644 B.J., et al. (2013). A functional CFTR assay using primary cystic fibrosis intestinal
645 organoids. Nat. Med. *19*, 939–945.

646 13. Schutgens, F., Rookmaaker, M.B., Margaritis, T., Rios, A., Ammerlaan, C., Jansen, J.,
647 Gijzen, L., Vormann, M., Vonk, A., Viveen, M., et al. (2019). Tubuloids derived from
648 human adult kidney and urine for personalized disease modeling. Nat. Biotechnol. *37*,
649 303–313.

650 14. Sachs, N., Papaspyropoulos, A., Zomer-van Ommen, D.D., Heo, I., Böttinger, L., Klay,
651 D., Weeber, F., Huelsz-Prince, G., Iakobachvili, N., Amatngalim, G.D., et al. (2019).
652 Long-term expanding human airway organoids for disease modeling. EMBO J. *38*,
653 e100300.

654 15. Berkers, G., van Mourik, P., Vonk, A.M., Kruisselbrink, E., Dekkers, J.F., de Winter-
655 de Groot, K.M., Arets, H.G.M., Marck-van der Wilt, R.E.P., Dijkema, J.S.,
656 Vanderschuren, M.M., et al. (2019). Rectal Organoids Enable Personalized Treatment
657 of Cystic Fibrosis. Cell Rep. *26*, 1701-1708.e3.

658 16. Dekkers, J.F., Berkers, G., Kruisselbrink, E., Vonk, A., de Jonge, H.R., Janssens, H.M.,
659 Bronsveld, I., van de Graaf, E.A., Nieuwenhuis, E.E.S., Houwen, R.H.J., et al. (2016).
660 Characterizing responses to CFTR-modulating drugs using rectal organoids derived
661 from subjects with cystic fibrosis. Sci. Transl. Med. *8*, 344ra84.

662 17. van Mourik, P., Beekman, J.M., and van der Ent, C.K. (2019). Intestinal organoids to
663 model cystic fibrosis. Eur. Respir. J. *54*.

664 18. Ramalho, A.S., Fürstová, E., Vonk, A.M., Ferrante, M., Verfaillie, C., Dupont, L.,
665 Boon, M., Proesmans, M., Beekman, J.M., Sarouk, I., et al. (2020). Correction of
666 CFTR function in intestinal organoids to guide treatment of Cystic Fibrosis. Eur.
667 Respir. J.

668 19. Guimbellot, J.S., Leach, J.M., Chaudhry, I.G., Quinney, N.L., Boyles, S.E., Chua, M.,
669 Aban, I., Jaspers, I., and Gentzsch, M. (2017). Nasospheroids permit measurements of
670 CFTR-dependent fluid transport. JCI insight *2*.

671 20. Brewington, J.J., Filbrandt, E.T., LaRosa, F.J. 3rd, Ostmann, A.J., Strecker, L.M.,
672 Szczesniak, R.D., and Clancy, J.P. (2018). Detection of CFTR function and modulation

673 in primary human nasal cell spheroids. J. Cyst. Fibros. Off. J. Eur. Cyst. Fibros. Soc.
674 *17*, 26–33.

675 21. Liu, Z., Anderson, J.D., Deng, L., Mackay, S., Bailey, J., Kersh, L., Rowe, S.M., and
676 Guimbellot, J.S. (2020). Human Nasal Epithelial Organoids for Therapeutic
677 Development in Cystic Fibrosis. Genes (Basel). *11*.

678 22. Keating, D., Marigowda, G., Burr, L., Daines, C., Mall, M.A., McKone, E.F., Ramsey,
679 B.W., Rowe, S.M., Sass, L.A., Tullis, E., et al. (2018). VX-445-Tezacaftor-Ivacaftor in
680 Patients with Cystic Fibrosis and One or Two Phe508del Alleles. N. Engl. J. Med.
681 *379*, 1612–1620.

682 23. Mou, H., Vinarsky, V., Tata, P.R., Brazauskas, K., Choi, S.H., Crooke, A.K., Zhang,
683 B., Solomon, G.M., Turner, B., Bihler, H., et al. (2016). Dual SMAD Signaling
684 Inhibition Enables Long-Term Expansion of Diverse Epithelial Basal Cells. Cell Stem
685 Cell *19*, 217–231.

686 24. Eenjes, E., Mertens, T.C.J., Buscop-van Kempen, M.J., van Wijck, Y., Taube, C.,
687 Rottier, R.J., and Hiemstra, P.S. (2018). A novel method for expansion and
688 differentiation of mouse tracheal epithelial cells in culture. Sci. Rep. *8*, 7349.

689 25. Hynds, R.E., Gowers, K.H.C., Nigro, E., Butler, C.R., Bonfanti, P., Giangreco, A.,
690 Prêle, C.M., and Janes, S.M. (2018). Cross-talk between human airway epithelial cells
691 and 3T3-J2 feeder cells involves partial activation of human MET by murine HGF.
692 PLoS One *13*, e0197129.

693 26. Feng, W., Guo, J., Huang, H., Xia, B., Liu, H., Li, J., Lin, S., Li, T., Liu, J., and Li, H.
694 (2015). Human Normal Bronchial Epithelial Cells: A Novel In Vitro Cell Model for
695 Toxicity Evaluation. PLoS One *10*, e0123520.

696 27. Fulcher, M.L., Gabriel, S., Burns, K.A., Yankaskas, J.R., and Randell, S.H. (2005).
697 Well-differentiated human airway epithelial cell cultures. Methods Mol. Med. *107*,
698 183–206.

699 28. Gray, T.E., Guzman, K., Davis, C.W., Abdullah, L.H., and Nettesheim, P. (1996).
700 Mucociliary differentiation of serially passaged normal human tracheobronchial
701 epithelial cells. Am. J. Respir. Cell Mol. Biol. *14*, 104–112.

702 29. Namkung, W., Yao, Z., Finkbeiner, W.E., and Verkman, A.S. (2011). Small-molecule
703 activators of TMEM16A, a calcium-activated chloride channel, stimulate epithelial
704 chloride secretion and intestinal contraction. FASEB J. Off. Publ. Fed. Am. Soc. Exp.
705 Biol. *25*, 4048–4062.

706 30. Pozo, A., Regnier, M., Lizotte, J., Martineau, C., Scorza, T., and Moreau, R. (2020).
707 Cyclic adenosine monophosphate-dependent activation of transient receptor potential
708 vanilloid 4 (TRPV4) channels in osteoblast-like MG-63 cells. Cell. Signal. *66*, 109486.

709 31. Genovese, M., Borrelli, A., Venturini, A., Guidone, D., Caci, E., Viscido, G.,
710 Gambardella, G., di Bernardo, D., Scudieri, P., and Galietta, L.J. V (2019). TRPV4 and
711 purinergic receptor signalling pathways are separately linked in airway epithelia to
712 CFTR and TMEM16A chloride channels. J. Physiol. *597*, 5859–5878.

713 32. Kettle, R., Simmons, J., Schindler, F., Jones, P., Dicker, T., Dubois, G., Giddings, J.,
714 Van Heeke, G., and Jones, C.E. (2010). Regulation of neuregulin 1beta1-induced
715 MUC5AC and MUC5B expression in human airway epithelium. Am. J. Respir. Cell
716 Mol. Biol. *42*, 472–481.

717 33. Vermeer, P.D., Panko, L., Karp, P., Lee, J.H., and Zabner, J. (2006). Differentiation of
718 human airway epithelia is dependent on erbB2. Am. J. Physiol. Lung Cell. Mol.

719 Physiol. *291*, L175-80.

720 34. Gray, T., Coakley, R., Hirsh, A., Thornton, D., Kirkham, S., Koo, J.-S., Burch, L.,
721 Boucher, R., and Nettesheim, P. (2004). Regulation of MUC5AC mucin secretion and
722 airway surface liquid metabolism by IL-1beta in human bronchial epithelia. Am. J.
723 Physiol. Lung Cell. Mol. Physiol. *286*, L320-30.

724 35. Abdullah, L.H., Coakley, R., Webster, M.J., Zhu, Y., Tarran, R., Radicioni, G.,
725 Kesimer, M., Boucher, R.C., Davis, C.W., and Ribeiro, C.M.P. (2018). Mucin
726 Production and Hydration Responses to Mucopurulent Materials in Normal versus
727 Cystic Fibrosis Airway Epithelia. Am. J. Respir. Crit. Care Med. *197*, 481–491.

728 36. Gentzsch, M., Cholon, D.M., Quinney, N.L., Boyles, S.E., Martino, M.E.B., and
729 Ribeiro, C.M.P. (2018). The cystic fibrosis airway milieu enhances rescue of F508del
730 in a pre-clinical model. Eur. Respir. J. *52*.

731 37. Chen, G., Sun, L., Kato, T., Okuda, K., Martino, M.B., Abzhanova, A., Lin, J.M.,
732 Gilmore, R.C., Batson, B.D., O'Neal, Y.K., et al. (2019). IL-1β dominates the
733 promucin secretory cytokine profile in cystic fibrosis. J. Clin. Invest. *129*, 4433–4450.

734 38. Brouillard, F., Bouthier, M., Leclerc, T., Clement, A., Baudouin-Legros, M., and
735 Edelman, A. (2001). NF-kappa B mediates up-regulation of CFTR gene expression in
736 Calu-3 cells by interleukin-1beta. J. Biol. Chem. *276*, 9486–9491.

737 39. Balázs, A., and Mall, M.A. (2018). Role of the SLC26A9 Chloride Channel as Disease
738 Modifier and Potential Therapeutic Target in Cystic Fibrosis. Front. Pharmacol. *9*,
739 1112.

740 40. Pranke, I., Hatton, A., Masson, A., Flament, T., Le Bourgeois, M., Chedevergne, F.,
741 Bailly, C., Urbach, V., Hinzpeter, A., Edelman, A., et al. (2019). Might Brushed Nasal

742 Cells Be a Surrogate for CFTR Modulator Clinical Response? Am. J. Respir. Crit. Care
743 Med. *199*, 123–126.

744 41. Harris, C.M., Mendes, F., Dragomir, A., Doull, I.J.M., Carvalho-Oliveira, I., Bebok, Z.,
745 Clancy, J.P., Eubanks, V., Sorscher, E.J., Roomans, G.M., et al. (2004). Assessment of
746 CFTR localisation in native airway epithelial cells obtained by nasal brushing. J. Cyst.
747 Fibros. Off. J. Eur. Cyst. Fibros. Soc. *3 Suppl 2*, 43–48.

748 42. Stokes, A.B., Kieninger, E., Schögler, A., Kopf, B.S., Casaulta, C., Geiser, T.,
749 Regamey, N., and Alves, M.P. (2014). Comparison of three different brushing
750 techniques to isolate and culture primary nasal epithelial cells from human subjects.
751 Exp. Lung Res. *40*, 327–332.

752 43. Boj, S.F., Vonk, A.M., Statia, M., Su, J., Vries, R.R.G., Beekman, J.M., and Clevers,
753 H. (2017). Forskolin-induced Swelling in Intestinal Organoids: An In Vitro Assay for
754 Assessing Drug Response in Cystic Fibrosis Patients. J. Vis. Exp.

755 44. Dekkers, J.F., Alieva, M., Wellens, L.M., Ariese, H.C.R., Jamieson, P.R., Vonk, A.M.,
756 Amatngalim, G.D., Hu, H., Oost, K.C., Snippert, H.J.G., et al. (2019). High-resolution
757 3D imaging of fixed and cleared organoids. Nat. Protoc. *14*, 1756–1771.

758

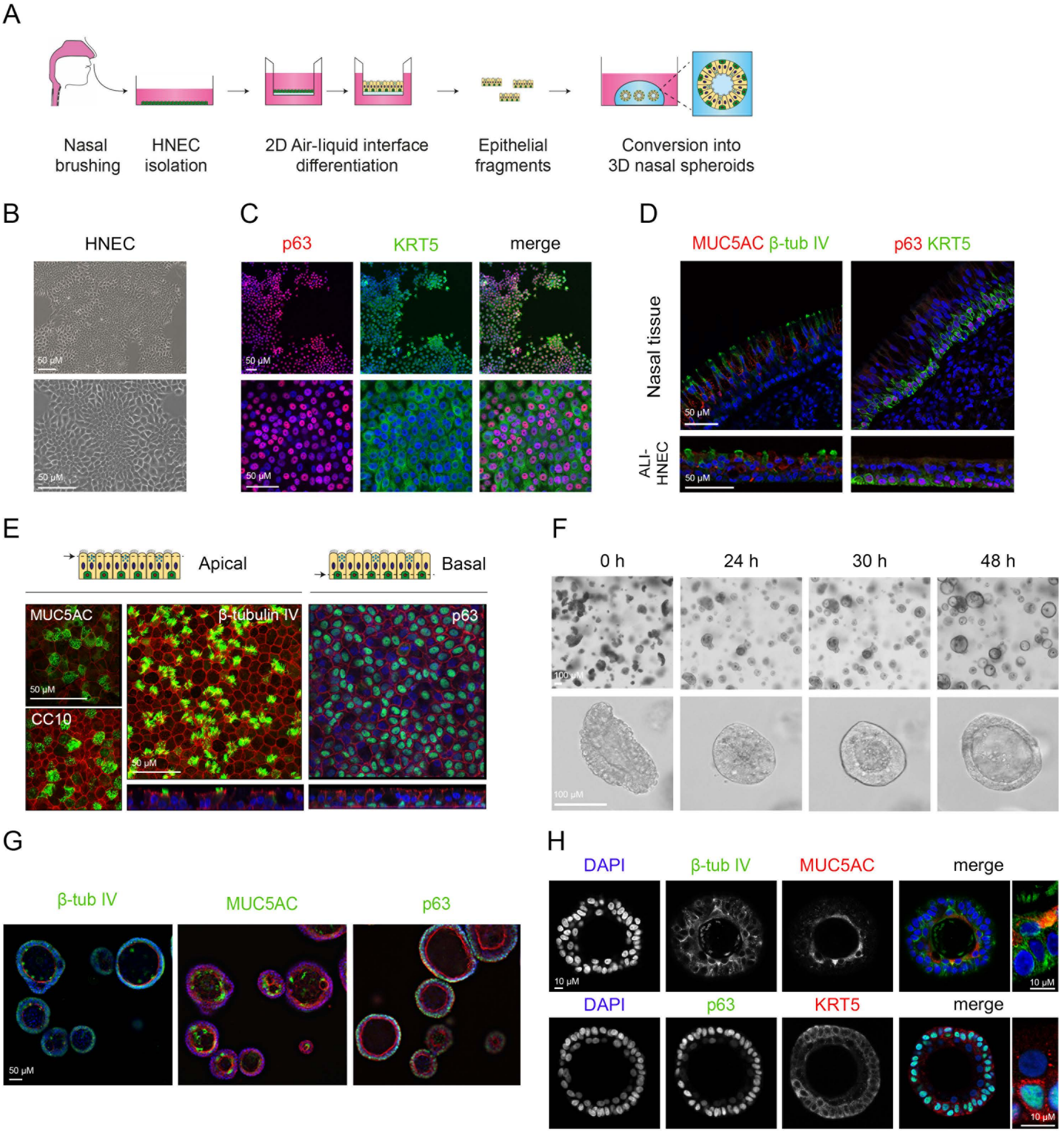
A
Nasal brushing
HNEC isolation
2D Air-liquid interface differentiation
Epithelial fragments
Conversion into 3D nasal spheroids
B
HNEC
50 µM
C
p63
KRT5
merge
D
MUC5AC β-tub IV
p63 KRT5
Nasal tissue
ALI-HNEC
E
Apical
Basal
MUC5AC
β-tubulin IV
p63
CC10
F
0 h
24 h
30 h
48 h
100 µM
G
β-tub IV
MUC5AC
p63
H
DAPI
β-tub IV
MUC5AC
merge
DAPI
p63
KRT5
merge
10 µM

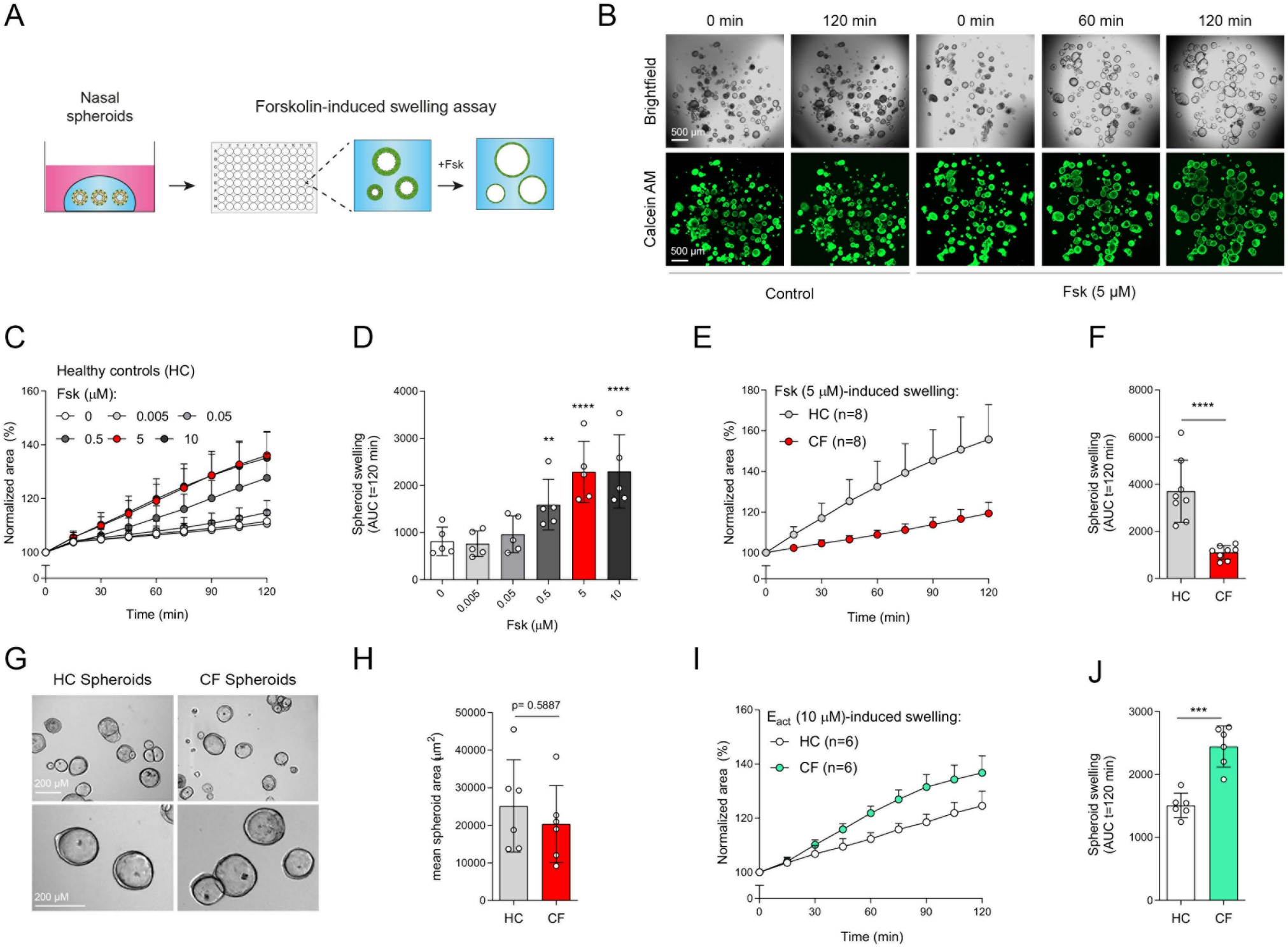
A
Nasal spheroids
Forskolin-induced swelling assay
+Fsk
B
0 min
120 min
0 min
60 min
120 min
Brightfield
Calcein AM
500 µm
Control
Fsk (5 µM)
C
Healthy controls (HC)
Fsk (µM):
0
0.005
0.05
0.5
5
10
Normalized area (%)
Time (min)
D
Spheroid swelling (AUC t=120 min)
Fsk (µM)
E
Fsk (5 µM)-induced swelling:
HC (n=8)
CF (n=8)
Normalized area (%)
Time (min)
F
Spheroid swelling (AUC t=120 min)
HC
CF
G
HC Spheroids
CF Spheroids
200 µM
H
p= 0.5887
mean spheroid area (µm²)
HC
CF
I
Eact (10 µM)-induced swelling:
HC (n=6)
CF (n=6)
Normalized area (%)
Time (min)
J
Spheroid swelling (AUC t=120 min)
HC
CF

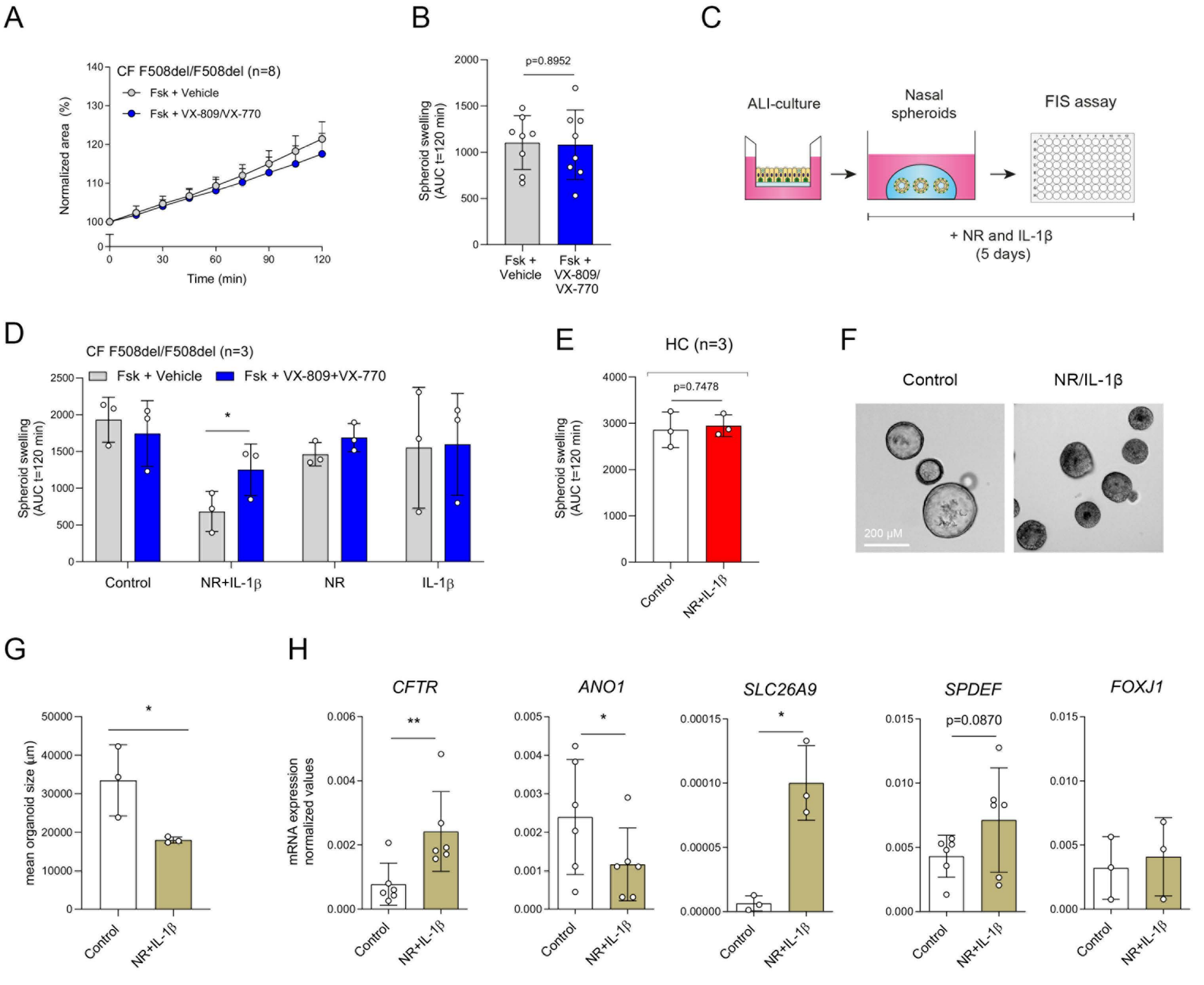
A
CF F508del/F508del (n=8)
Fsk + Vehicle
Fsk + VX-809/VX-770
Normalized area (%)
Time (min)
B
p=0.8952
Spheroid swelling (AUC t=120 min)
Fsk + Vehicle
Fsk + VX-809/ VX-770
C
ALI-culture
Nasal spheroids
FIS assay
+ NR and IL-1β (5 days)
D
CF F508del/F508del (n=3)
Fsk + Vehicle
Fsk + VX-809+VX-770
Spheroid swelling (AUC t=120 min)
Control
NR+IL-1β
NR
IL-1β
E
HC (n=3)
p=0.7478
Spheroid swelling (AUC t=120 min)
Control
NR+IL-1β
F
Control
NR/IL-1β
200 µM
G
mean organoid size (µm)
Control
NR+IL-1β
H
CFTR
ANO1
SLC26A9
SPDEF
FOXJ1
mRNA expression normalized values
p=0.0870
Control
NR+IL-1β

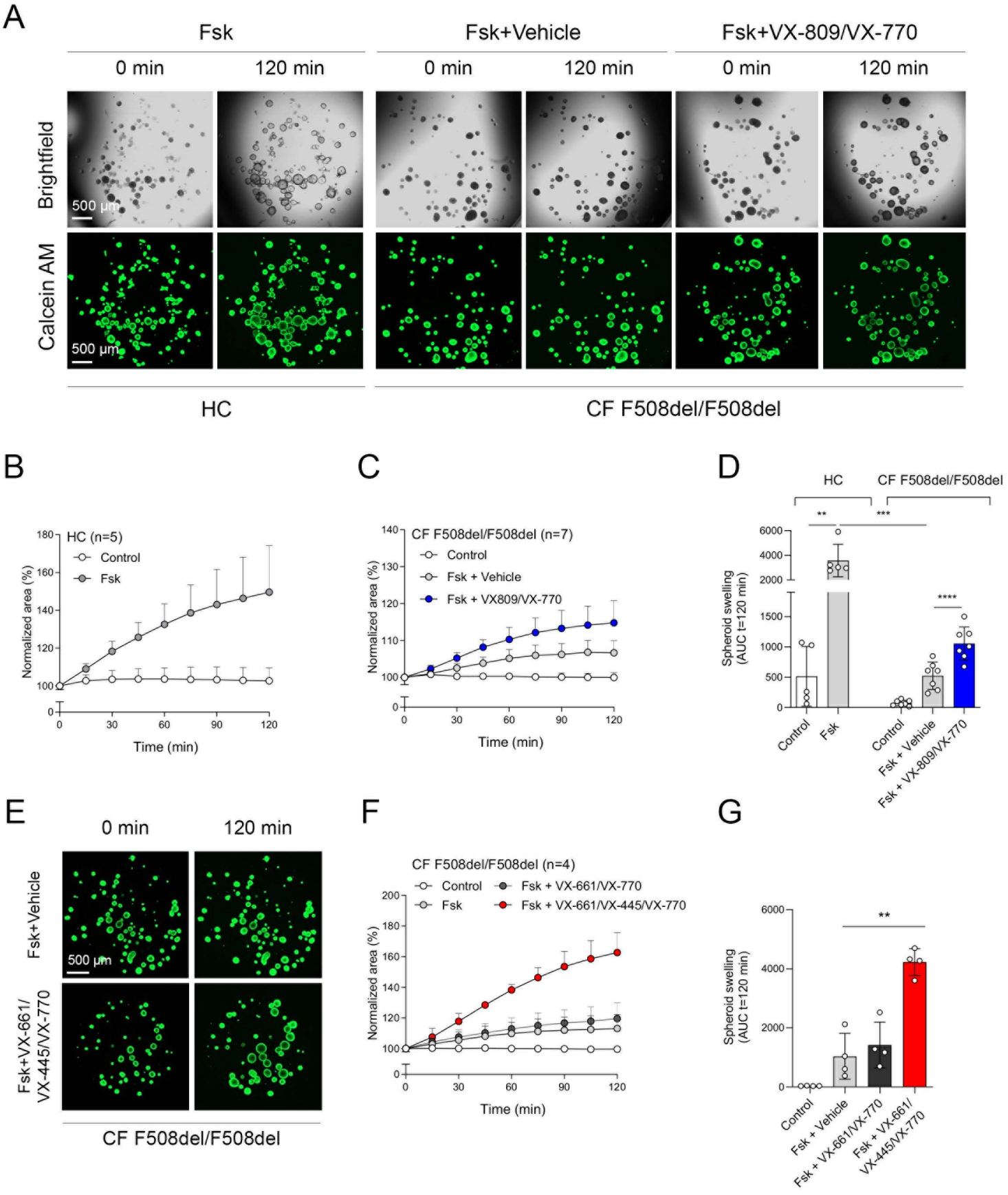
A
Fsk
Fsk+Vehicle
Fsk+VX-809/VX-770
0 min
120 min
Brightfield
Calcein AM
500 µm
HC
CF F508del/F508del
B
HC (n=5)
Control
Fsk
Normalized area (%)
Time (min)
C
CF F508del/F508del (n=7)
Control
Fsk + Vehicle
Fsk + VX809/VX-770
Normalized area (%)
Time (min)
D
HC
CF F508del/F508del
Spheroid swelling (AUC t=120 min)
Control
Fsk
Control
Fsk + Vehicle
Fsk + VX-809/VX-770
E
0 min
120 min
Fsk+Vehicle
Fsk+VX-661/ VX-445/VX-770
500 µm
CF F508del/F508del
F
CF F508del/F508del (n=4)
Control
Fsk
Fsk + VX-661/VX-770
Fsk + VX-661/VX-445/VX-770
Normalized area (%)
Time (min)
G
Spheroid swelling (AUC t=120 min)
Control
Fsk + Vehicle
Fsk + VX-661/VX-770
Fsk + VX-661/ VX-445/VX-770